Preservation of thalamocortical circuitry is essential for good recovery after cardiac arrest

Prejaas K. B. Tewarie [a,b,*], Marleen C. Tjepkema-Cloostermans[a,c], Romesh G. Abeysuriya[d], Jeannette Hofmeijer[a,e] and Michel J. A. M. van Putten [a,c]

aClinical Neurophysiology Group, University of Twente, 7522 NH Enschede, Netherlands
bSir Peter Mansfield Imaging Centre, School of Physics, University of Nottingham, NG7 2QX Nottingham, UK
cDepartment of Neurology and Clinical Neurophysiology, Medisch Spectrum Twente, 7512 KZ Enschede, Netherlands
dComputational Epidemic Modelling, Burnet Institute, 3004 Melbourne, Australia
eDepartment of Neurology, Rijnstate Hospital, 6815 AD Arnhem, Netherlands
*To whom correspondence should be addressed. Email: prejaas.tewarie@nottingham.ac.uk
Edited By: Stephen Fleming

Abstract

Continuous electroencephalographam (EEG) monitoring contributes to prediction of neurological outcome in comatose cardiac arrest survivors. While the phenomenology of EEG abnormalities in postanoxic encephalopathy is well known, the pathophysiology, especially the presumed role of selective synaptic failure, is less understood. To further this understanding, we estimate biophysical model parameters from the EEG power spectra from individual patients with a good or poor recovery from a postanoxic encephalopathy. This biophysical model includes intracortical, intrathalamic, and corticothalamic synaptic strengths, as well as synaptic time constants and axonal conduction delays. We used continuous EEG measurements from hundred comatose patients recorded during the first 48 h postcardiac arrest, 50 with a poor neurological outcome [cerebral performance category (CPC = 5)] and 50 with a good neurological outcome (CPC = 1). We only included patients that developed (dis-)continuous EEG activity within 48 h postcardiac arrest. For patients with a good outcome, we observed an initial relative excitation in the corticothalamic loop and corticothalamic propagation that subsequently evolved towards values observed in healthy controls. For patients with a poor outcome, we observed an initial increase in the cortical excitation-inhibition ratio, increased relative inhibition in the corticothalamic loop, delayed corticothalamic propagation of neuronal activity, and severely prolonged synaptic time constants that did not return to physiological values. We conclude that the abnormal EEG evolution in patients with a poor neurological recovery after cardiac arrest may result from persistent and selective synaptic failure that includes corticothalamic circuitry and also delayed corticothalamic propagation.

Keywords: electroencephalography, corticothalamic mean-field model, coma, cardiac arrest, biophysical modelling

---

Significance

The temporal evolution of brain activity, commonly measured by the electroencephalographam (EEG), serves as an important prognostic marker for neurological recovery of comatose patients after cardiac arrest. While early reappearance of brain activity is associated with a good recovery, other specific EEG abnormalities are associated with a poor recovery. The pathophysiological mechanisms underlying these EEG patterns in patients after cardiac arrest are poorly understood. Using a method to estimate parameters from a biophysical model, we shed light on the pathophysiological mechanisms underlying EEG evolution in these patients. We demonstrate that poor outcome predominantly results from persistent synaptic failure, especially between the cortex and the thalamus, and delayed propagation of activity between the cortex and thalamus.

Introduction

Continuous electroencephalographam (EEG) monitoring in the first 24 h after cardiac arrest has a pivotal role in prognostication in comatose survivors after cardiac arrest (1), allowing reliable prediction of neurological outcome in about 50% of the patients (2). Neurological prognostication not only depends on identification of specific EEG abnormalities but also on the evolution and timing of these abnormalities postcardiac arrest (3). In all

comatose patients directly after cardiac arrest, the EEG is severely disturbed and mostly suppressed. In patients with a good neurological outcome, EEG activity typically evolves towards continuous brain activity on time scales of 24 h (4, 5). A delayed (>24 h) evolution towards continuous activity is associated with a poorer outcome (1). Persistent suppression with or without synchronous bursts, or generalized periodic discharges (GPDs) on a flat background are invariably associated with a poor outcome (7, 2, 6).

While the clinical relevance of EEG phenomenology in postanoxic encephalopathy is well known, the underlying pathophysiological mechanisms of EEG patterns associated with poor or good outcome are incompletely understood. Only in extreme cases, the pathophysiology is relatively clear: if adenosine triphosphate (ATP) is depleted sufficiently long, irreversible loss of resting membrane potentials occurs, and cell swelling will follow, resulting in massive neuronal death accompanied by persistent isoelectric EEG (12, 11, 8, 10, 9). However, in the pathogenesis of rhythmic and periodic or diffusely slowed EEG, as observed in many patients with moderate to severe hypoxic/ischaemic injury, it is predominantly synaptic failure that results in these abnormal EEG patterns (14, 13, 9), where our understanding of selective dysfunction of excitatory or inhibitory synapses is incomplete (7).

Only a few studies have explored this role of synaptic damage in EEG abnormalities in postanoxic encephalopathy. These studies were mainly based on so-called mean-field models (15, 16). Several of these models can describe average postsynaptic membrane potentials of coupled excitatory and inhibitory cortical populations as a function of spike rates, synaptic strengths, and synaptic time constants. The voltage fluctuations of the excitatory cortical neurons can subsequently be used as a proxy for EEG registrations. A common approach for mean-field modeling is hypothesis-driven manipulations of model parameters (13, 17, 18). For instance, selective elimination of excitatory synapses from pyramidal neurons to inhibitory neurons in a mean-field model showed GPDs that resembled empirically observed GPDs (17). Another modeling study on postanoxic encephalopathy showed that a gradual recovery of synaptic strength led to an EEG evolution that was consistent with empirical data, i.e. suppressed activity, followed by burst-suppression and continuous activity. Here, the amount of suppression was a function of the "hypoxic burden" (depth and duration). This "hypoxic burden" determined whether continuous activity could be retrieved as final stage (13).

Though very informative in providing a qualitative explanation of the evolution of EEG abnormalities, these previous approaches cannot retrieve subject specific trajectories of model parameters, such as temporal changes in synaptic properties. This contrasts with a recent approach using a corticothalamic mean-field model where model parameters are retrieved by finding the best fit between the observed and model's power spectrum for every point in time, enabling real-time tracking of mean-field parameters over time for each individual patient (19). The model has successfully been used to track sleep stages in terms of temporal evolution of physiological parameters (19). The use of this parameter estimation method yields time-resolved trajectories of both excitatory and inhibitory synaptic strengths and synaptic time constants. This method also estimates nonsynaptic parameters such as corticothalamic conduction delays. It therefore allows us to test the hypothesis that EEG abnormalities in patients after cardiac arrest can be completely explained by isolated selective synaptic failure. Here, we use this method to study pathophysiological mechanisms of EEG pattern evolution in comatose patients with a postanoxic encephalopathy. Lastly, in order to analyze how specific estimated parameters are for EEG recordings from comatose survivors of cardiac arrest, we also apply our method and compare our results to EEG recordings from comatose survivors of traumatic brain injury (TBI).

Results

We used EEG data from 100 healthy control subjects to obtain reference values for all estimated model parameters. We selected EEGs from 50 comatose survivors of cardiac arrest with a poor outcome and 50 patients with a good outcome from our previously published dataset (7, 3). We only selected patients who developed a discontinuous or continuous EEG within 48 h after cardiac arrest (see methods section for rationale). Fig. 1A shows an example of EEG segments of 7 s from two patients at $t = 12$ and $t = 24$ h after cardiac arrest as example. The EEG in the upper panel shows an evolution from burst-suppression at 12 h after cardiac arrest to a continuous EEG with alpha activity (8–13 Hz) at 24 h after cardiac arrest from a patient with a good outcome. The EEG in the lower panel shows an evolution from burst-suppression at 12 h after cardiac arrest to a nearly continuous EEG with slower theta rhythms (4–8 Hz) at 24 h after cardiac arrest from a patient with a poor outcome. For every subject, we derived a power spectrum for every hour of their EEG recording until 48 h postcardiac arrest. Fig. 1B shows the evolution of the power spectrum for the same patients as in Fig. 1A with a good (upper panel) and a poor outcome (lower panel). The occurrence and a shift of the spectral peak in the alpha band is clearly visible in the patient with a good outcome (purple corresponds to $t = 12$ h and light green to $t = 48$ h). A similar evolution is visible in the patient with poor outcome, but the spectral peak remains in the theta band.

We employed a corticothalamic mean-field model that describes the mean membrane potential of four connected neuronal populations. Details of the model and the parameter estimation method can be found in the methods section. In brief, the model includes a cortical excitatory and cortical inhibitory population and a thalamic relay and reticular population (Fig. 1C). The postsynaptic membrane potential of a population modulates as a consequence of synaptic input mediated by the firing activity of presynaptic populations. The effect of the presynaptic input on the postsynaptic membrane potential depends on the mean number of synapses between the presynaptic b and postsynaptic population a (modeled as synaptic strength ν_{ab}) and on the closing and opening rate of synaptic channels characterized by the synaptic decay and rise constants (α and β). The average postsynaptic membrane potential is transformed at the cell bodies in a population, giving rise to the firing activity. This process results in propagation of activity in a closed loop between thalamic and cortical populations, where firing rate propagated between the thalamus and the cortex is delayed by t_0. Using ν_{ab}, we can disentangle this corticothalamic system to a purely cortical loop or gain X, a corticothalamic gain Y and a intrathalamic gain Z. The cortical gain is defined in terms of the ratio of cortical excitatory versus cortical inhibitory synaptic strengths.

Using a Markov chain Monte Carlo random walk method (19–21), we estimated the temporal evolution of these six biophysical parameters X, Y, Z, α, β, and t_0 from consecutive EEG power spectra from every subject over the course of 48 h. Fig. 1D shows the goodness-of-fit in terms of χ^2 for patients with a good and a poor outcome, respectively. No significant difference was observed in model prediction accuracy between these two groups (Mann–Whitney U $p > 0.05$).

For every parameter, the mean and standard error across subjects is depicted in Fig. 1D, alongside the distribution of values from healthy controls (blue violin plots). Differences between groups across time points were assessed by nonparametric permutation testing (22). For the cortical gain X, we see a separation between the means and their standard error for both groups in the initial phase ($t < 24$ h after cardiac arrest), followed by an overlap between the means and their standard error for later phases ($t > 24$ h after cardiac arrest). Hence, there is a higher cortical excitation-inhibition ratio in patients with a poor outcome in the initial phase of $t < 24$ after cardiac arrest. Permutation testing
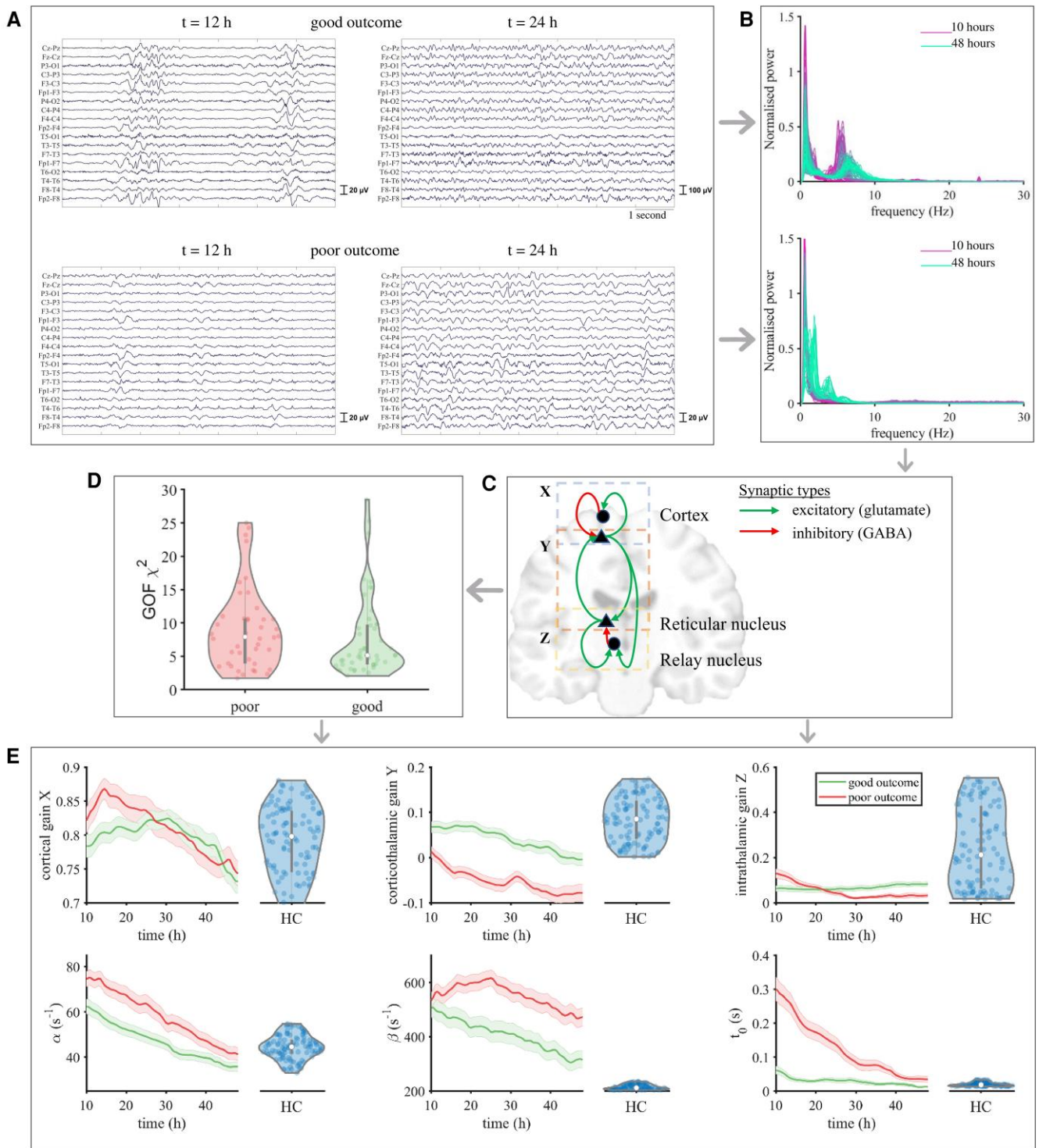
Fig. 1. Estimating model parameters from EEG data. Panel A) shows two EEG segments from two subjects at t = 12 h and t = 24 h after cardiac arrest. Upper panel shows EEG data from one subject with good outcome, lower panel shows EEG data from a different subject with poor outcome. The consecutive power spectra for the same subjects are demonstrated in panel B). Power spectra from every hour are depicted, starting at 10 h after cardiac arrest (purple/dark colour) to 48 h after cardiac arrest (light green/light colour). Panel C) shows the corticothalamic mean-field model. There are two populations in the thalamus and cortex. Red lines correspond to inhibitory synaptic connections and green lines to excitatory synaptic connections. Panel D) shows the distributions (violin plots) of the goodness-of-fit (GOF) χ^2 for the two groups. Here, every dot corresponds to the mean GOF across time points for one subject. Panel E) shows the mean and standard error for all parameters, alongside the distribution of values from healthy controls (violin plots). Key findings in patients with a poor outcome are (1) an initial high cortical excitation-inhibition ratio; (2) a persistent loss of corticothalamic gain Y, i.e. relative excess of corticothalamic inhibition; (3) slow synaptic responses (high values for α and β); (4) slow propagation of activity between the thalamus and cortex (high values for t_0). Abbreviations: cortical gain X, corticothalamic gain Y, intrathalamic gain Z, synaptic decay constant α, synaptic rise constant β, and time delay of propagation between thalamus and the cortex t_0.

across all time points, however, showed no significant difference between groups ($p > 0.05$). For the corticothalamic gain Y, there is no overlap between groups across all time points, resulting in a significant difference ($p = 0.03$). Y values for patients with a good outcome overlapped with the distribution of Y values from healthy controls, which was not the case for patients with a poor outcome. For patients with a poor outcome, Y is negative in contrast to positive values of Y for patients with a good outcome. This reflects dominance of inhibition in the corticothalamic loop in patients with a poor outcome; positive values correspond to dominance of excitation in the corticothalamic loop. For the intra-thalamic gain Z, there was a upward trend for patients with a good outcome and a downward trend for patients with a poor outcome. However, there was no significant difference between groups ($p > 0.05$). For both patients with a good and poor outcome, the values of Z overlapped with the distribution of Z from healthy controls.

For the synaptic decay time α, we observed a significant difference between patients with a good and a poor outcome ($P < 0.001$). Patients with a good outcome had lower values of α, with the tendency to reach the range of values of α of healthy control subjects at an earlier stage than patients with a poor outcome. For the synaptic rise time β, there was a significant difference between groups ($P < 0.001$), with a steeper negative curve for patients with a good outcome and a tendency towards values of β from healthy controls. Lower values for α and β correspond to a synaptic response with smaller width, hence the ability to generate faster rhythms. The parameter t_0 is the only parameter indicative of axonal integrity and captures the conduction velocity between the thalamus and the cortex. There was a significant difference in t_0 values between groups ($P < 0.001$). Patients with a good outcome had overall shorter delays than patients with poor outcome. Around $t = 48\,$h, patients with a good outcome had values of t_0 that strongly overlapped with values of t_0 from healthy control subjects.

We have also investigated the specificity of our findings by applying our parameter estimation method to a different group of comatose patients with evident EEG slowing. A previously reported and fairly large sample of patients with TBI were included for this purpose (23). Results are shown in the supplementary material Fig. S1. In brief, in contrast to comatose survivors of cardiac arrest, comatose survivors of TBI show much slower temporal evolution of estimated parameters for the first 48 h after trauma. There was lower cortical excitation X, as well as higher intrathalamic gain Z in the patients with TBI. Furthermore, EEG slowing in TBI patients was also characterized by preserved conduction velocity between the thalamus and the cortex.

Discussion

We used a biophysical mean-field model to study the pathophysiology of EEG abnormalities in patients with a postanoxic encephalopathy and show that poor outcome is associated with an initial high cortical excitation-inhibition ratio, relative inhibition in the corticothalamic loop, overall slow recovery of time scales of synaptic responses and longer delays in propagation of activity between the thalamus and cortex. Patients with a good outcome showed excitation in the corticothalamic loop, faster recovery of time scales of synaptic responses, and faster propagation of activity between the cortex and thalamus with values that were essentially similar to those of healthy control subjects. Our findings show that poor outcome results from failure in synaptic recovery as well as from impaired axonal propagation (difference in t_0 between groups).

In patients with a poor outcome, there was a higher cortical excitation-inhibition ratio in the first 24 h after cardiac arrest compared to patients with a good outcome. This difference normalized after 24 h. The higher cortical excitation-inhibition ratio is supported by clinical observations such as increased risk of electrographic or clinical seizures in this patient population (24, 25), or high incidence of GPDs, which may result from increased cortical excitability (7, 26). Note that not all parameters showed convergence around 48 h after cardiac arrest. This could be related to the fact that it takes more time for a complete normalization of the EEG to occur, and hence also more time for the parameters to converge.

Our model suggests persistent corticothalamic synaptic failure in patients with a poor recovery. This finding is in line with animal work and postmortem data showing selective damage of reticular neurons in the thalamus after cardiac arrest (28, 27), leading to excessive activity in the thalamus. Since efficient communication between the thalamus and the cortex depends on phasic inhibition or cyclic suppression in the thalamus (29), allowing short temporal windows of sensitivity to synaptic input, tonic activity in the thalamus could disrupt this loop and hence could relate to decreased corticothalamic synaptic strength. Other postmortem work also suggests that patients with thalamic damage had EEG abnormalities associated with poor outcome (11). Moreover, integrity of corticothalamic synapses is associated with the ability to generate alpha oscillations (31, 30) and usually emerge from the model if $Y > 0$ (31). This was in line with our empirical findings, as patients with a good outcome in general had $Y > 0$. Patients with a poor outcome had negative values for Y, which is usually associated with slower delta and theta activity (31). We also show that the integrity of corticothalamic synaptic connections are more important to distinguish good from poor outcome than intracortical interactions. This is in agreement with the so-called mesocircuit hypothesis (33, 32). This hypothesis postulates that recovery of consciousness after severe brain injury (both postanoxic encephalopathy and TBI) strongly depends on recovery of excitatory activity in a thalamocortical circuit.

Failure of synaptic transmission is a well-known consequence of cerebral hypoxia or ischemia (34, 13). Here we report longer synaptic rise and decay times for all synapses in patients with a poor outcome. These parameters correspond to opening and closing times of ligand-gated channels in the synapse and can be translated to a synaptic impulse response function (35). The opening and closing times of ligand-gated channels strongly relate to the frequency response of postsynaptic membranes and longer synaptic rise and decay times correspond to the inability to generate faster rhythms (alpha and beta) in patients with a poor outcome (36). Results agree with previous animal and in vitro work showing longer postsynaptic potentials after hypoxia (38, 37). This is probably the result of long-term potentiation (LTP) mediated by upregulation of N-methyl-D-aspartate (NMDA)-receptors due to excess of extracellular glutamate after hypoxia (39). We show that opening times of ligand-gated synaptic channels are shorter and normalize faster in patients with a good outcome compared to poor outcome, but still differs from values from healthy controls. Hence, further recovery of the EEG may depend on reversing LTP (13).

Propagation of activity between the cortex and thalamus was severely delayed for patients with a poor outcome. Longer delays in the corticothalamic loop generally result in slower theta and delta rhythms (36), consistent with our empirical findings in this group with a poor outcome. For patients with a good outcome, there was evolution towards a conduction delay comparable to

that of healthy control subjects. Previous work showed that mild hypoxia induces isolated synaptic failure with intact heights and shapes of the action potential, suggesting intact axonal membrane functioning (34). Other in vitro work has shown that oligodendrocytes are vulnerable to hypoxia, resulting in defects in myelination due to hypoxia (40, 41). Animal work has also shown that anoxia can lead to detachment of perinodal oligodendrocyte-axon loops, and thus cause axonal injury (42). Our finding of longer conduction delays between the cortex and thalamus in patients with a poor outcome and is suggestive of myelination defects rather than axonal damage. This is in line with findings from diffusion tensor imaging studies showing increased radial diffusivity in patients after cardiac arrest, suggestive of myelination defects (43).

An important issue regarding our estimated parameters is the uniqueness and specificity of our solution in this specific patient population. Are our estimated parameters informative for this specific type of pathology or will any EEG slowing irrespective of type of pathology or even EEG slowing during sleep fit to these same set of parameters? Previous work using our parameter estimation method has demonstrated that slow wave activity during non-rapid eye movement sleep (NREM) sleep does not fit one-to-one to the estimated parameters that we found for our patients after cardiac arrest (44, 19): decay time of the synaptic response α during NREM is slower than for our patient group, and the intrathalamic gain Z during NREM is lower as well. This relates to the sensitivity of our parameter estimation method to changes in both the slope of the power spectrum as well as height of the spectral peaks. During NREM sleep, delta waves have usually high amplitude, which will influence the slope of the power spectrum, and hence, also the estimated parameters. In addition, our results from TBI underscore that EEG slowing in any pathology may not necessarily map onto the same set of parameter values. For some parameters, we found distinct values for the two groups (X, Z, t_0). While for other parameters, there was an overlap in parameter values, e.g. corticothalamic gain Y, which could indicate final common pathways in coma, also emphasized by the mesocircuit hypothesis (33).

Some limitations apply to our work. First, synaptic rise and decay times were aggregated for all populations (excitatory, inhibitory, and thalamic). This simplification is probably not justified by the underlying neurophysiology but was required to reduce the number of estimated parameters. Second, we ignored spatial effects. Input to our model were power spectra averaged across all electrodes. While it may be more realistic to estimate sensor specific parameters, the EEG after cardiac arrest does not show high regional specificity but rather homogeneous activity over different electrodes. Furthermore, this would have resulted in an excess of parameters. Third, our model cannot disentangle presynaptic and postsynaptic effects. Last, in order to estimate underlying neurophysiological parameters, we did not employ the full nonlinear model, but a linearized version of the model. This is probably not critical as previous work suggests that many empirical phenomenon can be captured using the linearized version of the mean-field model (36, 44).

In conclusion, we have provided insight into potential pathophysiological mechanisms of EEG abnormalities in postanoxic encephalopathy. We show that these EEG abnormalities are mostly reflective of synaptic failure, though not limited to isolated synaptic failure as poor outcome was also accompanied with longer axonal conduction delays between the cortex and thalamus, probably reflecting myelination defects. Preservation of

thalamocortical synaptic connections, propagation of neuronal activity between the cortex and thalamus, and normalization of synaptic responses appear crucial for evolution of the EEG associated with good outcome in patients with postanoxic encephalopathy. This framework and these findings pave the way to detect synaptic failure in individual patients.

Methods
Study population
We selected EEGs from 50 comatose survivors of cardiac arrest with poor outcome and 50 patients with good outcome from our previously published dataset (7, 3). Selection was based on three criteria: a cerebral performance category (CPC) score of either 1 (poor outcome) or 5 (good outcome) at six months after cardiac arrest to maximize contrast between groups; CPC of 1 only as a result of postanoxic coma (and not, for example, as a result of multiple organ or systemic failure); and an evolution towards a continuous or discontinuous EEG at 48 h postcardiac arrest. This last criterium is to ensure that we avoid mixing up different EEG abnormalities and corresponding pathways in patients with poor outcome. For example, the pathophysiological underpinnings burst-suppression with identical bursts may be different from the pathophysiological underpinnings of a continuous EEG with GPDs. Hence, EEGs with the following abnormalities were excluded during our selection: GPDs on an iso-electric background, burst-suppression as final stage, rhythmic activity (>2.5 Hz) or periodic activity (0.5–2.5 Hz), and a suppressed EEG.

To obtain a reference for all estimated biophysical parameters, we used eyes-closed EEG data from 100 healthy controls.

EEG preprocessing
Continuous EEG recordings were used from patients with cardiac arrest admitted to the ICU. Nineteen electrodes (either silver/silver chloride cup or subdermal wire) were placed according to the 10–20 international system. A Neurocenter EEG system with Refa or SAGA amplifiers (TMSi, Netherlands) was used, recording at a sample frequency of 256 Hz. EEG data until 48 h after cardiac arrest were used for further analysis using the longitudinal bipolar montage. These EEG data were further preprocessed using a zero-phase sixth-order Butterworth bandpass filter of 0.5–40 Hz. We used a semi-automated algorithm to detect and remove artifacts within windows of 10 s in the common average. Artifacts included empty channels, channels with large peaks or noise (amplitude $\geq 200\,\mu V$ or $\leq -200\,\mu V$ and variance $\geq 1400\,\mu V^2$ or $\leq 1\,\mu V^2$), or muscle artifacts. In addition, we used independent component analysis to detect and remove the electrocardiogram (ECG) artifact after visual inspection of individual components (45). After preprocessing, we computed a power spectrum for every hour and every channel and averaged across channels. Power spectra were computed using Welch's method with windows of 10 s with 5 s overlap.

Corticothalamic mean-field model
We employed a corticothalamic mean-field model (46, 47, 36), which describes the aggregate activity of a neuronal population in terms of their firing rate ϕ_a and mean membrane potential V_a with $a \in \{e, i, r, s\}$. The corticothalamic mean-field model encompasses two cortical populations (excitatory e and inhibitory i) and two thalamic populations (relay s and reticular r). The membrane potential of a population fluctuates $V_a(t)$ as a result of the

incoming firing rate $\phi_a(t)$ from other population and/or itself according to

$$\left(\frac{1}{\alpha\beta}\frac{d^2}{dt^2} + \left(\frac{1}{\alpha} + \frac{1}{\beta}\right)\frac{d}{dt} + 1\right)V_a(t) = \sum_{a'} v_{aa'}\phi_{a'}(t) + \sum_b v_{ab}\phi_b(t - t_0/2). \quad (1)$$

The constants α and β refer to the synaptic rise and decay constants, $v_{aa'}$ and v_{ab} to the synaptic strength between populations, where v_{ab} refers to synaptic strength between the thalamic and cortical populations. Propagation between thalamic and cortical populations is delayed by t_0. At the cell body, the membrane potential V_a is transformed into a firing rate using a sigmoid function

$$Q_a(t) = \frac{Q_{max}}{1 + \exp(-(V_a(t) - \theta)/\sigma)}. \quad (2)$$

The mean firing rate is further temporally damped using the following expression:

$$\left(\frac{1}{\gamma_a^2}\frac{d^2}{dt^2} + \frac{2}{\gamma_a}\frac{d}{dt} + 1\right)\phi_a(t) = Q_a(t), \quad (3)$$

with γ_a being the temporal damping rate, based on $\gamma = v_a/r_a$, where v_a is the propagation velocity and r_a is the mean range of axons. For inhibitory, relay, and reticular populations, $\gamma_a \approx \infty$, hence $\phi_a(t) = Q_a(t)$.

Estimation of model parameters

Model power spectrum

Parameter estimation for nonlinear models remains challenging. For example, error of estimated parameters near critical points or bifurcations can have severe effect on the expected behavior of the model. Equations 1–3 describe the full nonlinear model, which are first transformed to a linear model using linearization around a stable fixed point. Linearization is achieved by expressing the sigmoid function (Eq. 2) that transforms $V_a(t)$ into $Q_a(t)$ as Taylor expansion and retaining only the term containing the first derivative ρ_a evaluated at the fixed point. Details can be found in Ref. (19). Using the derivative ρ_a, we can express the synaptic strengths as gain parameters in the linear regime $G_{ab} = \rho_a v_{ab}$. These gain parameters can be transformed to three gain parameters describing the cortical X, corticothalamic Y, and intrathalamic loop gains

$$X = \frac{G_{ee}}{1 - G_{ei}}, \quad Y = \frac{G_{ese} + G_{esre}}{(1 - G_{srs})(1 - G_{ei})}, \quad Z = -G_{srs}\frac{\alpha\beta}{(\alpha+\beta)^2}. \quad (4)$$

Following this, the linear system in time domain can be rewritten in Fourier domain from which we can express an analytical expression for the power spectrum $P(w)$ as a function of frequency ω

$$P(w) = \frac{P_0}{|1 + Z'L^2|^2}\left(\frac{1}{|q^2|}\right)^2. \quad (5)$$

P_0 is a normalization constant (47) and q follows from the dispersion relation described in Ref. (19)

$$q^2 r_e^2 = \left(1 - \frac{i\omega}{\gamma}\right)^2 - X - \frac{Y(1 + Z')}{1 + Z'L^2}e^{i\omega t_0}. \quad (6)$$

Z' follows from a transformation of Z

$$Z' = Z\frac{(\alpha+\beta)^2}{\alpha\beta}, \quad (7)$$

and L follows from the transformation of the second-order differential operator describing the synaptic response (Eq. 1) in Fourier domain, which can be interpreted as a low-pass filter depending on the synaptic parameters α and β

$$L(\omega) = \frac{1}{(1 - i\omega/\alpha)}\frac{1}{(1 - i\omega/\beta)}. \quad (8)$$

Activity in pericranial muscles results in electromyogram (EMG) artifacts on the EEG, for which we need to account, hence, $P_{total}(\omega) = P(\omega) + P_{EMG}(\omega)$.

Fitting model parameters

The parameter set $\mathbf{x} = [X, Y, Z, \alpha, \beta, t_0, P_{EMG}]$ is estimated from EEG data by minimizing the error between the experimentally obtained power spectrum P_{exp} and model power spectrum $P_{total}(\mathbf{x})$ expressed as

$$\chi^2 = \sum_j W_j\left|\frac{P_{total}(\mathbf{x}) - P_{exp}}{P_{exp}}\right|^2, \quad (9)$$

where j indexes the frequency bins. The weights W_j ensure equal weighting for every frequency decade and is proportional to $1/f$. As parameter space is very large, we restrict parameter values to neurophysiologically plausible values [see Ref. (19) for values]. The χ^2 statistic is further transformed into a likelihood function

$$L(\mathbf{x}) = \exp\left[\frac{-\chi^2(\mathbf{x})}{2}\right]. \quad (10)$$

Hence, minimizing the error translates into maximizing this likelihood function. Now, the Metropolis–Hastings algorithm is used to generate a probability distribution for each parameter using a Markov chain random walk (20, 21). Details of the algorithm can be found in Ref. (19). For every subject, we run the Metropolis–Hastings algorithm to obtain model parameters for individual power spectra. The random walk is initialized by parameters obtained from a large database of healthy control subjects (44). This initialization will generally not affect the final output, but it affects the time of convergence. For every subsequent step in the random walk, the likelihood for this step is computed using Eq. 10. A new random proposed set is generated. The likelihood of this new set of parameters is again computed using Eq. 10. If these new parameters have a higher probability, this step is accepted and used to sample the probability distribution. Otherwise a random number is drawn from a uniform distribution. If this random number is smaller than the ratio of the probability of the new parameters to the old parameters, accept the step for sampling the probability distribution. If this random number is bigger than the ratio of the probability of the new parameters to the old parameters, then this step is not accepted. This procedure is repeated many times until there is no iterative change in the sampled probability distribution. Fitting a sequence of spectra at successive times would require to track temporal changes in parameter values. If we assume that the power spectrum does not change drastically for consecutive time points t_i and t_{i+1}, then we can use Bayes's theorem to inform our fit for t_{i+1} using estimated parameters from t_i as prior information.

Statistics

We used nonparametric permutation testing to test significance between groups of patients with a good and poor outcome (22). We tested whether a parameter across time points was significantly different between groups. We did not test for significance between groups for every time point separately to avoid a multiple testing problem. For every time dependent parameter $x_{sjg}(t)$, with

parameter index j, we computed the mean across subjects s for every group g denoted as $\langle x_{jg}(t) \rangle = (1/50) \sum_{s=1}^{50} x_{sjg}(t)$. We subsequently used the sum of the squared difference between group g (good outcome) and group g' (poor outcome) as test statistic $T_j = \sum_t \left(\langle x_{jg}(t) \rangle - \langle x_{jg'}(t) \rangle \right)^2$. Following this, we randomly permuted group membership 10,000 times and computed the test statistic for every realization to generate a null-distribution. The genuine value of the test statistic T_j was subsequently compared to the null-distribution and was considered to be significant if this would lie in the two 2.5% tail-ends of the null-distribution ($p < 0.05$). We performed in total six statistical tests (parameters X, Y, Z, α, β, t_0). All statistics were performed in MATLAB R2021a.

Acknowledgments

Supplementary material

Supplementary material is available at *PNAS Nexus* online.

Funding

Authors' contributions

Contribution of all authors is listed here: study design/conceptualization (P.K.B.T., M.J.A.M.vP.), data analysis/formal analysis (P.K.B.T., M.J.A.M.vP.), methodology/development method pipeline (R.G.A.), software (R.G.A.), data interpretation (P.K.B.T., M.C.T.C., R.G.A., J.H., M.J.A.M.vP.), data curation (M.C.M.C.), visualization (P.K.B.T.), writing manuscript (P.K.B.T., M.J.A.M.vP.), editing manuscript (P.K.B.T., M.C.T.C., R.G.A., J.H., M.J.A.M.vP.), supervision (J.H., M.J.A.M.vP.).

Data availability

Code for the parameter estimation method can be found on https://github.com/BrainDynamicsUSYD/braintrak, which includes explanation of the method on the wiki page https://github.com/BrainDynamicsUSYD/braintrak/wiki.

References

1 Sandroni C, *et al.* 2020. Prediction of poor neurological outcome in comatose survivors of cardiac arrest: a systematic review. *Intensive Care Med.* 46(10):1803–1851.

2 Hofmeijer J, *et al.* 2015. Early EEG contributes to multimodal outcome prediction of postanoxic coma. *Neurology.* 85(2):137–143.

3 Tjepkema-Cloostermans MC, *et al.* 2015. Electroencephalogram predicts outcome in patients with postanoxic coma during mild therapeutic hypothermia. *Crit Care Med.* 43(1):159–167.

4 Jørgensen EO, Holm S. 1998. The natural course of neurological recovery following cardiopulmonary resuscitation. *Resuscitation.* 36(2):111–122.

5 Sandroni C, *et al.* 2022. Prediction of good neurological outcome in comatose survivors of cardiac arrest: a systematic review. *Intensive Care Med.* 48(4):389–413.

6 Ruijter BJ, *et al.* 2019. Early electroencephalography for outcome prediction of postanoxic coma: a prospective cohort study. *Ann Neurol.* 86(2):203–214.

7 Ruijter BJ, van Putten MJAM, Hofmeijer J. 2015. Generalized epileptiform discharges in postanoxic encephalopathy: quantitative characterization in relation to outcome. *Epilepsia.* 56(11): 1845–1854.

8 Dijkstra K, Hofmeijer J, van Gils SA, van Putten MJAM. 2016. A biophysical model for cytotoxic cell swelling. *J Neurosci.* 36(47): 11881–11890.

9 Hofmeijer J, van Putten MJAM. 2012. Ischemic cerebral damage: an appraisal of synaptic failure. *Stroke.* 43(2):607–615.

10 Nutma S, Le Feber J, Hofmeijer J. 2021. Neuroprotective treatment of postanoxic encephalopathy: a review of clinical evidence. *Front Neurol.* 12:614698.

11 van Putten MJAM, *et al.* 2019. Postmortem histopathology of electroencephalography and evoked potentials in postanoxic coma. *Resuscitation.* 134:26–32.

12 Zandt B-J, ten Haken B, Gert van Dijk J, van Putten MJAM. 2011. Neural dynamics during anoxia and the "wave of death". *PLoS ONE.* 6(7):e22127.

13 Ruijter BJ, Hofmeijer J, Meijer HGE, van Putten MJAM. 2017. Synaptic damage underlies EEG abnormalities in postanoxic encephalopathy: a computational study. *Clin Neurophysiol.* 128(9): 1682–1695.

14 van Putten MJAM, Hofmeijer J. 2016. EEG monitoring in cerebral ischemia: basic concepts and clinical applications. *J Clin Neurophysiol.* 33(3):203–210.

15 Coombes S. 2010. Large-scale neural dynamics: simple and complex. *NeuroImage.* 52(3):731–739.

16 Deco G, Jirsa VK, Robinson PA, Breakspear M, Friston K. 2008. The dynamic brain: from spiking neurons to neural masses and cortical fields. *PLoS Comput Biol.* 4(8):e1000092.

17 Tjepkema-Cloostermans MC, Hindriks R, Hofmeijer J, van Putten MJAM. 2014. Generalized periodic discharges after acute cerebral ischemia: reflection of selective synaptic failure? *Clin Neurophysiol.* 125(2):255–262.

18 Victor JD, Drover JD, Conte MM, Schiff ND. 2011. Mean-field modeling of thalamocortical dynamics and a model-driven approach to EEG analysis. *Proc Natl Acad Sci USA.* 108(Suppl_3): 15631–15638.

19 Abeysuriya RG, Robinson PA. 2016. Real-time automated EEG tracking of brain states using neural field theory. *J Neurosci Methods.* 258:28–45.

20 Metropolis N, Rosenbluth AW, Rosenbluth MN, Teller AH, Teller E. 1953. Equation of state calculations by fast computing machines. *J Chem Phys.* 21(6):1087–1092.

21 Rosenthal JS, *et al.* 2011. Optimal proposal distributions and adaptive MCMC. In Brooks S, Gelman A, Jones G, Meng X-L, editors. Handbook of Markov chain Monte Carlo. 4(10.1201). Boca Raton (FL): Chapman & Hall/CRC.

22 Nichols TE, Holmes AP. 2002. Nonparametric permutation tests for functional neuroimaging: a primer with examples. *Hum Brain Mapp.* 15(1):1–25.

23 Tewarie P, *et al.* 2023. Early EEG monitoring predicts clinical outcome in patients with moderate to severe traumatic brain injury. *NeuroImage: Clin.* 37:103350.

24 Rossetti AO, *et al.* 2007. Status epilepticus: an independent outcome predictor after cerebral anoxia. *Neurology.* 69(3):255–260.

25 Ruijter BJ, *et al.* 2022. Treating rhythmic and periodic EEG patterns in comatose survivors of cardiac arrest. *N Engl J Med.* 386(8):724–734.

26 Barbella G, *et al.* 2020. Prediction of regaining consciousness despite an early epileptiform EEG after cardiac arrest. *Neurology*. 94-(16):e1675–e1683.

27 Ross DT, Graham DI. 1993. Selective loss and selective sparing of neurons in the thalamic reticular nucleus following human cardiac arrest. *J Cereb Blood Flow Metab*. 13(4):558–567.

28 Shoykhet M, *et al.* 2012. Thalamocortical dysfunction and thalamic injury after asphyxial cardiac arrest in developing rats. *J Neurosci*. 32(14):4972–4981.

29 Lőrincz ML, Kékesi KA, Juhász G, Crunelli V, Hughes SW. 2009. Temporal framing of thalamic relay-mode firing by phasic inhibition during the alpha rhythm. *Neuron*. 63(5):683–696.

30 Hindriks R, van Putten MJAM. 2013. Thalamo-cortical mechanisms underlying changes in amplitude and frequency of human alpha oscillations. *Neuroimage*. 70:150–163.

31 Roberts JA, Robinson PA. 2012. Corticothalamic dynamics: structure of parameter space, spectra, instabilities, and reduced model. *Phys Rev E*. 85(1):011910.

32 Edlow BL, Claassen J, Schiff ND, Greer DM. 2021. Recovery from disorders of consciousness: mechanisms, prognosis and emerging therapies. *Nat Rev Neurol*. 17(3):135–156.

33 Schiff ND. 2010. Recovery of consciousness after brain injury: a mesocircuit hypothesis. *Trends Neurosci*. 33(1):1–9.

34 Hofmeijer J, Mulder ATB, Farinha AC, van Putten MJAM, le Feber J. 2014. Mild hypoxia affects synaptic connectivity in cultured neuronal networks. *Brain Res*. 1557:180–189.

35 Rennie CJ, Robinson PA, Wright JJ. 2002. Unified neurophysical model of EEG spectra and evoked potentials. *Biol Cybern*. 86(6): 457–471.

36 Robinson PA, *et al.* 2001. Prediction of electroencephalographic spectra from neurophysiology. *Phys Rev E*. 63(2):021903.

37 Miyazaki S, *et al.* 1993. Post-ischemic potentiation of schaffer collateral/ca1 pyramidal cell responses of the rat hippocampus in vivo: involvement of n-methyl-d-aspartate receptors. *Brain Res*. 611(1):155–159.

38 Urban L, Neill KH, Crain BJ, Nadler JV, Somjen GG. 1989. Postischemic synaptic physiology in area ca1 of the gerbil hippocampus studied in vitro. *J Neurosci*. 9(11):3966–3975.

39 Szatkowski M, Attwell D. 1994. Triggering and execution of neuronal death in brain ischaemia: two phases of glutamate release by different mechanisms. *Trends Neurosci*. 17(9):359–365.

40 Dewar D, Underhill SM, Goldberg MP. 2003. Oligodendrocytes and ischemic brain injury. *J Cereb Blood Flow Metab*. 23(3):263–274.

41 Waxman SG, Black JA, Ransom BR, Stys PK. 1994. Anoxic injury of rat optic nerve: ultrastructural evidence for coupling between Na^+ influx and Ca^{2+}-mediated injury in myelinated CNS axons. *Brain Res*. 644(2):197–204.

42 Lyons SA, Kettenmann H. 1998. Oligodendrocytes and microglia are selectively vulnerable to combined hypoxia and hypoglycemia injury in vitro. *J Cereb Blood Flow Metab*. 18(5):521–530.

43 Laitio R, *et al.* 2016. Effect of inhaled xenon on cerebral white matter damage in comatose survivors of out-of-hospital cardiac arrest: a randomized clinical trial. *JAMA*. 315(11):1120–1128.

44 Abeysuriya RG, Rennie CJ, Robinson PA. 2015. Physiologically based arousal state estimation and dynamics. *J Neurosci Methods*. 253:55–69.

45 Hyvarinen A. 1999. Fast and robust fixed-point algorithms for independent component analysis. *IEEE Trans Neural Netw*. 10(3): 626–634.

46 Freyer F, *et al.* 2011. Biophysical mechanisms of multistability in resting-state cortical rhythms. *J Neurosci*. 31(17):6353–6361.

47 Robinson PA, Rennie CJ, Rowe DL. 2002. Dynamics of large-scale brain activity in normal arousal states and epileptic seizures. *Phys Rev E*. 65(4):041924.